DOI: 10.15480/882.9346

Eighth International Symposium on Marine Propulsors
smp'24, Berlin, Germany, March 2024

An Investigation of Free-surface Effects on the Dynamics of Two-dimensional Oscillating Foil Thrusters in Tandem

D.B.S. Lopes[1], G. Vaz[2,3], J.A.C. Falcão de Campos[1], A.J.N.A. Sarmento[4]

[1]Instituto Superior Técnico, Av. Rovisco Pais 1, 1049-001 Lisbon, Portugal
[2]blueOASIS, Ericeira Business Factory, R. Prudêncio Franco da Trindade 4, 2655-344 Ericeira, Portugal
[3]Department of Civil, Maritime and Environmental Engineering, University of Southampton, UK
[4]WavEC – Offshore Renewables, Edifício Diogo Cão, Doca de Alcântara Norte, 1350-352 Lisbon, Portugal

ABSTRACT

The present work investigates free-surface effects on the dynamics of tandem oscillating foils in two-dimensional flow. The study comprises the cases in infinite domain, with and without an incident wave. A CFD solver with a URANS approach is used to model the flow around the tandem foil and the effects of the free-surface. A robust deforming grid method is used for body motion modelling, enabling large motions of the foils. Results of wake patterns and forces acting on the foils are presented for a high performance configuration. A complementary study uses a semi-analytical model based on Theodorsen unsteady theory. This formulation is extended to allow for the application to large motions and the interaction of both foils, including free-surface effects, and incident waves. The case of the tandem foil in waves shows very promising results. The high performance configuration reached high values of thrust and propulsive efficiency with increases in thrust of 38% when compared with the sum of two isolated single foils.

Keywords

Oscillating hydrofoils; Wave propulsion; Tandem foil; Hydrofoil modelling; CFD

1 INTRODUCTION

The ocean waves have long been considered as a potential source of energy for marine propulsion. Today, due to the widespread concern over the environment and global warming, there is a revived interest in wave powered boats using oscillating hydrofoils. Various researchers have successfully implemented oscillating foils in proof-of-concept prototype vehicles, as in the case of commercializing wave propelled ASVs (Autonomous Surface Vehicle) Liquid Robotics' WaveGlider and MOST's Autonaut (Wu et al., 2020). Also, recent interest in wave assisted propulsion of ships has led to the installation of foils on several vessels.

These efforts to develop practical solutions to wave powered propulsion systems may benefit from a large body of research that examined the operation of oscillating foils from a more theoretical approach. Lighthill (1960) was a pioneer in applying the fundamental hydrodynamic principles to the study of fish swimming. Wu (1971) and Wu & Chang (1975) addressed the thrust generation of an oscillating hydrofoil advancing in waves, but neglected the effect of the free-surface and the solid bottom. In four reports, Isshiki (1982a,b) and Isshiki and Murakami (1983, 1984) presented theoretical and experimental research on thrust generation of a hydrofoil advancing in waves. Their work provided the basic analytical framework to describe the interaction of an oscillating foil with waves. Silva and Yamaguchi (2012) used a commercially available CFD (RANS) code to study a two-dimensional hydrofoil oscillating harmonically in heave and pitch under the influence of free-surface waves. Simulation results were found to be in good agreement with the experimental results in Isshiki and Murakami (1984).

Researchers from the National Technical University of Athens (NTUA) carried out considerable numerical work in this field (Belibassakis & Filippas 2015; Filippas et al. 2018). They numerically investigated the hydrodynamic performance of flapping foils for ship propulsion, underneath the free-surface, employing panel methods. There was good agreement with the results in Silva and Yamaguchi (2012). Furthermore, Bøckmann and Steen from the Norwegian University of Science and Technology (NTNU) performed an experimental investigation to determine the effect of fixed wave foils on ship motion and propulsion (Bøckmann & Steen 2013, 2016), as well as the effect of control methods of oscillating motion on the performance of foils (Bøckmann & Steen 2014).

A promising approach to enhance the concept of single-foil propulsion involves in-line tandem flapping foils, i.e. a configuration of two parallel hydrofoils, one after the other, to mitigate unbalanced forces and potentially increase thrust and efficiency by utilizing the energy in the wake of the forward foil. As previously suggested by studies on live fish, investigations on tandem oscillating foil propulsors have proven that, with a proper distance

between two adjacent foils, the energy of previously shed vortices can be effectively utilized to increase the thrust generation (e.g. Zhu et al. 2012; Deng et al. 2007). Muscutt et al. (2014) from the University of Southampton presented the results of a comprehensive series of 2D numerical simulations of tandem foils in heave and pitch, in infinite domain. While the results have demonstrated the potential to improve thrust production and efficiency (Lagolopoulos 2020), the extent of the phase-spacing-frequency parameter space that has been explored is very limited. Other studies by Joshi & Mysa (2021) concerned the effect of chord-spacing ratio on propulsive forces and the mechanisms of vortex interaction, also in infinite domain. Xie et al (2017) used CFD to investigate a tandem foil mounted beneath the keel of a catamaran, in head waves.

Because of the complexity of nonlinear oscillatory hydrodynamics, studies of active tandem foil propulsors in waves are very scarce. The objective of this paper is to present first results with methods that attempt to capture the main physical processes acting on the tandem foil arrangement, allowing the understanding of the flow dynamics as well as the prediction of forces and moments involved. To this end we use the CFD code ReFRESCO which has been already verified and validated for applications with moving foils (Fernandes et al. 2016) and waves (Klaij et al. 2018).

In addition, and under the assumption that each foil interacts independently with the waves and that the foil-to-foil interaction can be accounted for by neglecting the free surface, a simple semi-analytical model based on the linear superposition of the different effects is investigated in its ability to predict thrust and efficiency.

The present paper is structured as follows: Section 2 describes the CFD model; governing equations, the flow solver, computational domain and boundary conditions, grids, numerical settings are presented. In Section 3 we describe the semi-analytical method. The results are discussed in Section 4 and conclusions are summarized in Section 5.

2 CFD MODEL

2.1 Governing Equations

The governing equations are the conservation of mass equation,

$$\partial\rho/\partial t + \nabla.(\rho \boldsymbol{v}) = 0 \qquad (1)$$

and the momentum equation, formulated as the Navier-Stokes equation

$$\rho\, \partial \boldsymbol{v}/\partial t + \rho(\boldsymbol{v}.\nabla)\boldsymbol{v} = -\nabla p + \rho \boldsymbol{g} + \nabla.\tau \qquad (2)$$

Here $\boldsymbol{v}$ denotes the velocity vector and τ the viscous stress tensor (Mewes 2021). These equations form a set of coupled, nonlinear partial differential equations, and their solution assuming incompressible flow gives the velocity and pressure fields. In this work for turbulent flows, the unsteady RANS model is adopted, and the Reynolds stresses are modelled with the k-ω Shear Stress Transport (SST) turbulence model version 2003 (Menter et al. 2003), commonly-used for maritime applications. This model includes two transport equations for the turbulent kinetic energy k and the dissipation rate per unit kinetic energy ω, respectively:

$$\partial/\partial t\,(\rho k) + \nabla.(\rho \boldsymbol{v} k) = \nabla.[(\mu + \mu_t/\sigma_k)\nabla k] + S^k \qquad (3)$$

$$\partial/\partial t\,(\rho \omega) + \nabla.(\rho \boldsymbol{v} \omega) = \nabla.[(\mu + \mu_t/\sigma_\omega)\nabla \omega] + S^\omega \qquad (4)$$

where S^k, S^ω and μ_t definitions and remaining model constants can be found in Mewes (2021), Moukalled et al. (2016) and Pereira (2018). In order to deal with two-phase flows i.e. for modelling air-water interfaces, where each fluid is considered constant-density, governing equations are also required. For free-surface type flows, a volume-fraction (VOF) variable is modelled and transported, representing the proportions of air/water in any given cell. The diffusion or source/sink terms are neglected and the free-surface transport equation for the volume fraction α (water or air) reads

$$\int \partial/\partial t\, \alpha + \nabla.\alpha \boldsymbol{v} dV = 0 \qquad (5)$$

2.2 Numerical Solver

The calculations in this work are carried out with the CFD code ReFRESCO (2022). The equations are discretized using a finite-volume approach with cell-centred collocated variables, in strong-conservation form. A segregated approach is adopted to solve all transport equations. The pressure-velocity coupling is dealt with via the SIMPLE (Ferziger & Perić 2002; Patankar 1980) algorithm. The second-order Implicit 3rd Time Level scheme is used for time integration, momentum convection discretization uses the second-order Limited QUICK scheme (Hoekstra 1999), and turbulence equations the First-Order Upwind scheme (Ferziger & Peric 2002). VOF convective discretization uses ReFRESCO's Interface-Capturing Scheme (Klaij et al. 2018) or the Total Variation Diminishing SuperBee scheme (Roe 1985).

Diffusive fluxes are always considered using a second-order central discretization. Corrections for eccentricity and non-orthogonality are considered for all terms. The resulting linear system of equations is iteratively solved using pre-conditioners and solvers from the PETSc library (Balay et al. 2013).

2.3 Domain and Boundary Conditions

The flow around NACA0012 oscillating foils is calculated in a prismatic rectangular computational domain defined in a Cartesian coordinate system (x, y, z). The coordinate system is centred at the middle point of the hydrofoil's trailing edge, or the front foil's trailing edge in case of tandem configuration, with the x axis aligned with the streamwise flow, the y axis set in the vertical direction, and the z axis oriented with the foil's span. The computational domain includes the following boundaries: inlet and outlet planes located at x = -20c and x = 50c; bottom and top planes at y = $\pm$50c, and two lateral spanwise planes at z =$\pm$1c. After a few preliminary

simulations, these distances were considered sufficient to avoid the reflection of the pressure field at the boundaries.

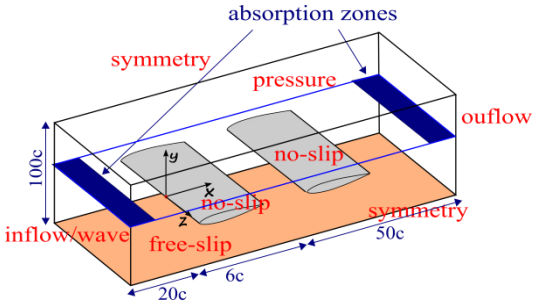

Figure 1: Schematic representation of the 2D computational domain and prescribed boundary conditions (not in scale).

The following boundary conditions are used:

At the foil surface an impermeability and no-slip conditions are applied. At the inlet an inflow wave boundary condition is set to simulate the effects of waves entering the domain and the freestream velocity. The wave is generated by prescribing both particle velocities and the volume fraction, as well as all other convective fluxes, with the result conforming to the Stokes wave theory to the fifth-order (Skjelbreia & Hendricksson 1960; Vaz et al. 2009). The components of the velocity vector are given by a Dirichlet boundary condition prescribed by a constant, while the pressure is extrapolated from the interior by approximations based on one-sided difference or extrapolations. At the outlet the usual assumption is that the normal derivatives of both velocity components vanish: The boundary values of the velocity components are determined by extrapolation from inner values. At the sidewalls symmetry conditions are used. The convective fluxes of all quantities are zero, and the normal gradient of the velocity component tangential to the symmetry boundary is also zero. The turbulent quantities and volume fraction are extrapolated from interior cells. At the top, the pressure is prescribed as constant. The velocities and other quantities are extrapolated from the interior as in the outflow boundary condition. At the bottom of the computational domain a free-slip condition is applied and the derivatives of all turbulence quantities with respect to y are set equal to zero.

The computational domain is schematically represented in Figure 1 together with the boundary conditions used.

Two wave absorption zones are prescribed to minimize wave reflections on the inlet and outlet. In these absorption zones the volume fraction is forced towards the undisturbed wave with a cosine absorption function (Perić & Abdel-Maksoud 2016). A trade-off in the maximum absorption value should be sought off since low values may lead to reflections from the boundary, while high values may cause reflection from the zone itself due to a too high forcing. It was found (Lopes 2022) that a 3.0c length damping zone was enough to avoid reflections.

2.4 Grid Layout and Deformation

Unstructured hexahedral meshes were generated for the selected computational domain using grid generation software Hexpress (Numeca 2022). Starting with a coarser base mesh two square regions of refinement were added: One around the perturbation damping area with 10 × 10c, the other covering the wake and then a circular refinement zone near the foil with a 1.1c radius. Two more regions of refinement were inserted, one at the foil trailing edge and the other at the leading edge, where the quantity gradients are greater. Figure 2 provides close-up zooms of the grid used in the simulation with heading waves. A viscous sub-layer was added in the cells adjacent to the foil surface targeting a non-dimensional wall distance $y^+ = 1$ (Schlichting & Gersten 2017).

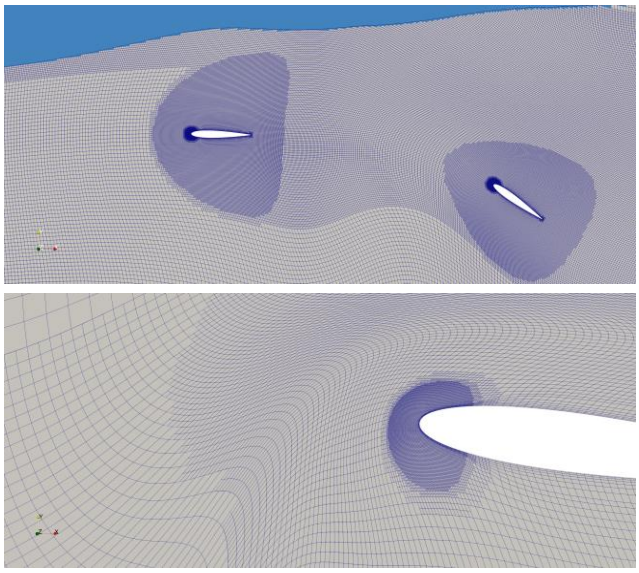

Figure 2: Example of grid refinement and deformation (a) general view; (b) detail of fore foil.

In order to model the rigid-body motion the deforming grid (DG) method based on the grid deformation of individual grid nodes (vertices) in combination with an imposed periodic rotation and/or translation of the hydrofoil in a fixed body reference system is used. To control deformation the Radial Basis Functions (RBF) method is employed, using interpolation functions to guarantee no grid deformation outside a defined support radius (Lombardi et al. 2013). Figure 2 present examples of the extent of grid deformation applied.

2.5 Estimation of Numerical Errors

Verification &Validation studies were extensively done in simpler cases of single and tandem foils in infinite domain (Lopes 2022; Lopes et al. 2023a) where the discretization error estimation used the procedure proposed by Eça and Hoekstra (2014). Based on these studies, and due to the complexity and computational costs of the present simulations, a choice was made about what grids to use.

3 SEMI-ANALYTICAL MODEL

In this section we consider the 2D problem of two submerged foils in tandem configuration, chord $c = 2a$

with a mean position at depth d, separated by a distance s, advancing with constant speed U and oscillating harmonically in heave and pitch at the same frequency, with inter-foil phase lag ϕ_t (fore foil leading the aft), in a heading sinusoidal gravity wave of amplitude a_0 and wavelength λ (wave number $k = 2\pi/\lambda$), in infinitely deep water. The present model is developed based on Wu's theory (1975) and Isshiki's work (1982a) for an unsteady hydrofoil in waves, neglecting free-surface effects.

For a single foil the classical ideal fluid theory assumes small disturbances to a uniform flow caused by the foil in heave and pitch motions in the presence of small amplitude incident surface waves. This allows the linearization of the flow boundary conditions. The thickness of the foil is assumed small compared to its chord and its effect is neglected, so that a symmetric foil is modelled as a flat plate. In unsteady flow vorticity is shed from the foil trailing edge due to change in time of the foil circulation. Outside the vortex wake shed from the foil trailing edge the flow is assumed irrotational (Newman 1978). The problem is specified by the Laplace equation in the fluid domain, the linearized kinematic boundary condition on the foil, the Kutta condition on the trailing edge, the infinite condition and the free-surface conditions, respectively. The origin of the coordinate system is considered to be at mid-chord of the foil in its average position (Figure 3).

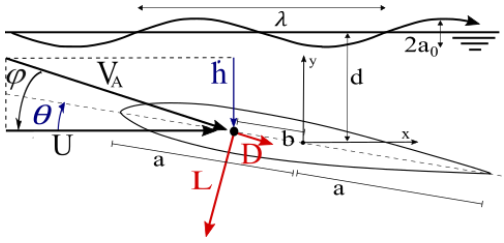

Figure 3: Model definition and coordinate system.

To solve this problem, considering first a single foil in infinite domain, the foil is modelled by a vortex distribution along the chord length, aligned with the x axis, and the wake is modelled by a straight line vortex distribution behind the foil, extending downstream to infinity (Theodersen 1935). In the linear theory the wake vorticity travels at the free stream speed (Newman, 1978). The vortex distribution on the foil specifies the difference in tangential velocities at the upper and lower sides of the foil, giving rise to a pressure difference between the two sides of the foil. The resultant pressure force or lift L has circulatory component L_C which is directed perpendicular to the incoming flow and a non-circulatory component L_{NC} related to the added mass, perpendicular to the foil.

Also, the foil is subject to a moment M. The linear theory limitation for large incident angles can be partially overcome by simply replacing U in lift definition by $V_A = U/\cos\varphi$. (Leishman 2006), where V_A is the apparent incident velocity and φ the angle of V_A with the advance speed U (Figure 3). The presence of incident waves will induce a small velocity perpendicular to the foil adding to the velocity induced by the foil motion. Isshiki and Murakami (1983) describe the interaction of the fluid and the foil in terms of the Theodorsen function and Bessel functions of first kind of first and second integer order.

It is assumed that the motion frequency is equal to the encounter frequency. The wave phase lag ϕ_w is defined to be at 0º when, at the wave crest, the foil is at its topmost position and about to go downwards, and the vertical component of the wave orbital velocity is also about to go downwards. Considering that for practical cases $ka << 1$ it is possible to simplify the Bessel functions to obtain (Lopes et al. 2023a):

$$\varphi(t) = \operatorname{atan}\left(ik_f h_0^* \left[1 - H_0^*\left(b^* - \frac{1}{2}\right)\theta_0^*\right] e^{i\omega_0 t}\right) \tag{6}$$

$$L_C = \frac{\rho a U^2\left[-2\pi C(k_f) h_0^*\right]}{\cos^2\varphi}\left\{ik_f\left[1 - H_0^* + \left(b^* - \frac{1}{2}\right)\theta_0^*\right] - \theta_0^*\right\} e^{i\omega_0 t} \tag{7}$$

$$L_{NC} = \frac{\rho a U^2[-\pi h_0^*]}{\cos^2\varphi}\{-k_f^2[1 - H_0^* + b^*\theta_0^*] - ik_f\theta_0^*\} e^{i\omega_0 t} \tag{8}$$

$$M_{NC} = \frac{2\rho a^2 U^2\left[-\frac{\pi h_0^*}{2}\right]}{\cos^2\varphi}\left\{k_f^2\left[b^*(1 - H_0^*) + \left(b^{*2} + \tfrac{1}{8}\right)\theta_0^*\right] - ik_f\left(b^* - \tfrac{1}{2}\right)\theta_0^*\right\} e^{i\omega_0 t} \tag{9}$$

$$M_C = -a\left(b^* + \frac{1}{2}\right) L_C \tag{10}$$

with

$$H_0^* = \frac{a_0^*}{h_0^*}\left(\frac{\sqrt{ka}}{\sqrt{2}F_r k_f}\right) e^{-(ka)2d^*} e^{i\phi_w} \tag{11}$$

In the previous equations the non-dimensional heave amplitude is $h_0^* = h_0/a$ and $b^* = b/a$. b is the x coordinate of the pitching axis relative to the origin at mid-chord, (leading edge negative). $d^* = d/c$ is the non-dimensional depth and $\theta_0^* = \theta_0/h_0^*$ the non-dimensional pitch amplitude. The reduced frequency is given by $k_f = \omega_0 a/U$. Since the foil is oscillating at encounter frequency, k_f is not independent of ka, and they are related by $k_f = ka + \sqrt{ka}/(\sqrt{2}F_r)$, where the Froude number is given by $F_r = U/\sqrt{gc}$.

For the tandem foil configuration we assume that the aft foil wake effect in the fore foil is minimal, with sufficient inter-foil distance (Epps et al. 2016). The fore foil effect on the aft foil is accounted in the following way: Firstly, the horizontal vortex advection velocity ratio $r_{va} = U_{for}/U$, accounts for the higher aft foil flow speed due to the jet of the fore foil. Epps et al. (2016) propose $r_{va} = 1.2$.

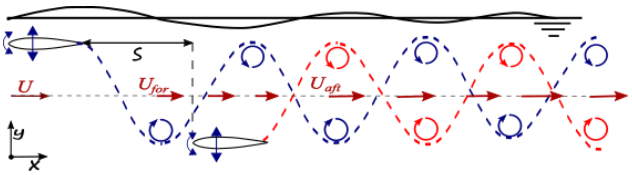

Figure 4: Simplified example for the tandem foil wake pattern. *U*, U_{for} and U_{aft} are the foil advance velocity, fore foil vortex advection velocity and aft foil vortex advection velocity, respectively.

Secondly, we postulate that there is a vertical velocity component induced on the aft foil by the fore foil vorticity that only affects the foil apparent inflow angle:

$$\varphi_2 = atan\left(ik_f h_0^* \left[1 + \left(b^* - \frac{1}{2}\right)\theta_0^*\right] - \frac{L_C^s/\rho a U^2}{2\pi(s^*+2)}\right) e^{i\omega_0 t}, \quad (12)$$

where $s^* = s/a$ and L_C^s the circulatory lift for a single foil that can be obtained from Equation (7). Moreover, it is assumed that the main additional effect of the tandem configuration is the interference of the two wakes. We also assume that the vortex shedding is independent for the two foils and the superimposition of the vortices shed by both foils starts on the trailing edge of the aft foil and continues downstream. Due to the linearity assumption, the effect of the two wakes can be added with respect to the aft foil. The circulatory lift of the aft foil in tandem configuration $L_{C,2}^t$ can then be expressed in terms of the circulatory lift of the single fore and aft foils (Lopes et al., 2023a), with heave and pitch amplitudes and heave-pitch phases set equal in both foils.:

$$L_{C,2}^t = L_C^s r_{va}^2 \left\{1 + \left[1 - \frac{E(k_f, s^*)}{C(k_f)}\right] e^{i[\phi_t - k_f(s^*+2)]}\right\} \quad (13)$$

$E(k_f, s^*)$ is given by:

$$E(k_f, s^*) \approx -\frac{2/\pi}{H_1^{(2)}(k_f) + iH_0^{(2)}(k_f)} \times \left[\int_{-(s^*+1)}^{-1} \frac{e^{-ik_f\xi}}{(\xi^2-1)^{1/2}} d\xi - 2.5538 {k_f}^{-0.649}\right] \quad (14)$$

with $H_n^{(2)}(k_f)$ being the Hankel functions of second kind (For details see Lopes et al. 2023b). Because the non-circulatory lift $L_{NC,2}^t$ does not depend on the wake, the formula presented for a single foil can be applied. This is also the case for the non-circulatory moment $M_{NC,2}^t$ and drag D_2^t. The circulatory moment of the aft foil $M_{C,2}^t$ can be easily obtained from Equation (10).

The total thrust, vertical forces and moment of the foil tandem system are the sum of the instantaneous forces on each foil.

$$F_x^t = \sum_{i=1,2} \left(-L_{C,i}^t \sin\varphi_i - L_{NC,i}^t \sin\theta_i + D_i^t \cos\varphi_i\right) \quad (15)$$

$$F_y^t = \sum_{i=1,2} \left(L_{C,i}^t \cos\varphi_i + L_{NC,i}^t \cos\theta_i + D_i^t \sin\varphi_i\right) \quad (16)$$

$$M^t = \sum_{i=1,2} \left(M_{Ci}^t + M_{NCi}^t\right) \quad (17)$$

To evaluate the viscous drag *D* expressions for the drag of a flat plate with corrections for thickness, angle of attack and separation (Hoerner 1965; Faltinse, 2005) are used. (For details see Lopes 2022).

4 RESULTS

Results of the instantaneous forces and the time-averaged thrust and efficiency are presented for the CFD calculations. We denote by $\bar{T}$ the time-averaged value of $-F_x(t)$ (negative horizontal force corresponds to positive thrust), and by $\bar{P}$ the average input power per cycle:

$$\bar{T} = -\frac{\omega_0}{2\pi}\int_0^{2\pi/\omega_0} F_x\, dt \quad (18)$$

$$\bar{P} = \frac{\omega_0}{2\pi}\left[\left|\int_0^{2\pi/\omega_0} F_y \dot{h}\, dt\right| + \int_0^{2\pi/\omega_0} M\dot{\theta} dt\right] \quad (19)$$

The propulsive efficiency, η_P, is defined to be the ratio of useful power over input power, as $\eta_P = U\bar{T}/\bar{P}$. The thrust coefficient is defined by $\bar{C}_T = \bar{T}/(0.5\rho c U^2)$.

Also relevant flow field visualizations of vorticity and velocity are presented, for two sets of test cases:

(1) Submerged tandem foil without incident waves
(2) Submerged tandem foil in heading waves

4.1 Submerged Tandem Foil without Incident Waves

Solely one simulation was run, using a grid of 530k cells and number of iterations per period n_t/T = 8333. For the current study we select a set of motion and parameters to allow comparison with the results of the tandem in an infinite domain previously studied in (Lopes et al. 2023a). The inter-foil phase lag ϕ_t = 180° is selected for a case with high performance so the positive interference of the wakes can be analysed. The motion parameters are shown in Table 1.

Figure 5 shows snapshots of the instantaneous vorticity and velocity fields of the tandem foil with free-surface and in infinite domain at high performance configuration.

In the high performance case, the aft foil is weaving in between the primary vortices that are shed from the fore foil. It is possible to see that this increases the strength of its vortices shed into the wake. These strong vortices become interspersed with the vortices shed from the fore foil forming vertical pairs and creating a double reversed BvK street. On the other hand, the interaction of the aft foil with the fore foil secondary vortices drives them out of the way in the wake, avoiding the drag effects that they cause in the isolated single foil.

Table 1: Simulation parameters for the submerged tandem foil test case without incident waves.

Parameter	Submerged	Infinite domain
Inflow velocity, U	1 m/s	1 m/s
Chord, c	1 m	1 m
Pitching axis, b^*	1/3-point	1/3-point
Heave amplitude, h_o	1.0 m	1.0 m
Pitch amplitude, θ_o	41.5° ($\alpha_0 \approx 10°$)	41.5° ($\alpha_0 \approx 10°$)
Pitch phase, ψ	90°	90°
Period, T	5.0 s ($S_t = 0.4$)	5.0 s ($S_t = 0.4$)
Submergence, d	1.25 m	-
Foil separation, s	4 m	4 m
Inter-foil phase lag, ϕ_t	180°	180°
Reynolds number, Re	40 000	40 000

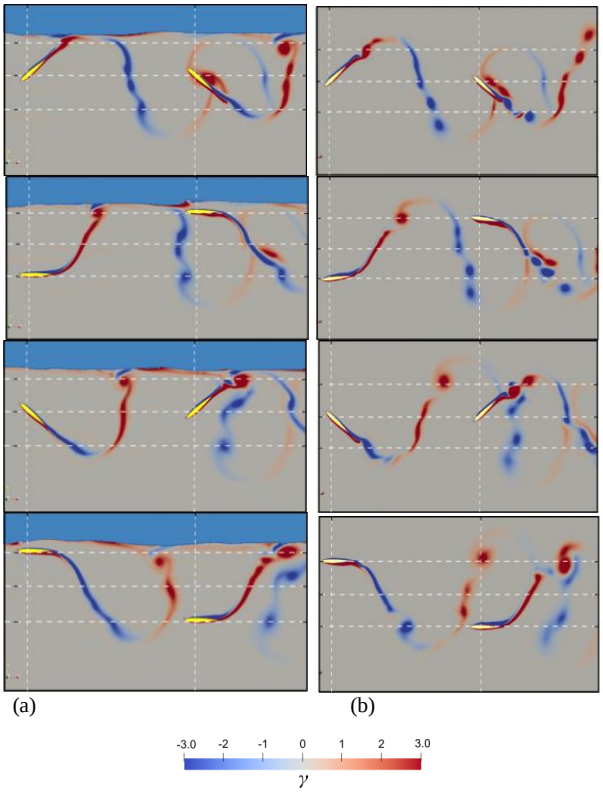

Figure 5: Snapshots of vorticity for a tandem of NACA0012 foils in high performance (a) with free-surface and (b) in infinite domain at cycle increments of t/T = ¼. Clockwise vorticity is indicated with blue, and anticlockwise with red. The vertical lines show the location of 1/3 point pitching axis of the foils, and the horizontal lines show the mid foil position and the upper and lower limits of heave motion.

With the presence of the free-surface the interaction of the fore foil with the free-surface in the end of the upstroke, causes the increase of the positive pressure on the lower surface of the foil, augmenting the positive vorticity and resulting in the shedding of a stronger counter clockwise leading edge vortex (color in red).

Figure 6 shows the instantaneous thrust, vertical and moment coefficients for both fore and aft foils. It is possible to see the augmentation of the aft thrust coefficient relatively to the fore foil, especially in the aft foil upstroke (t/T=0 to 0.25).

Table 2 presents the results for the average thrust coefficient for the fore, aft foils and total tandem and compares it with results of the tandem foil in infinite domain previously studied.

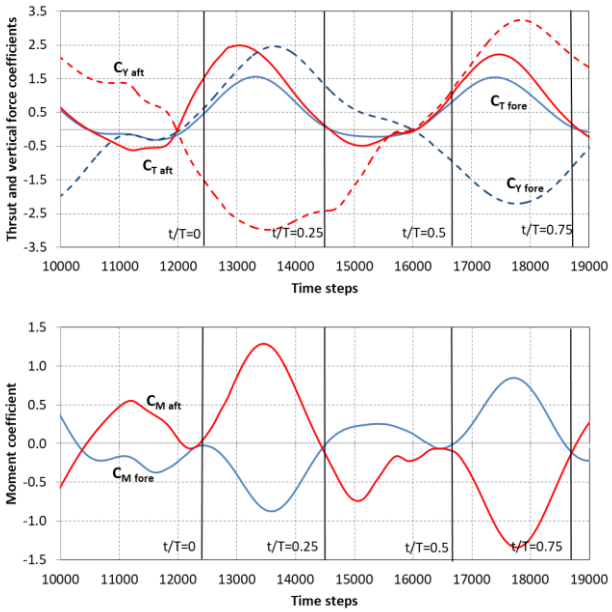

Figure 6: (a) Thrust and vertical force and (b) moment coefficients instantaneous values for the forward foil and aft foil in the submerged tandem test case without incident waves.

Table 2: Results of the average thrust coefficient for the submerged tandem foil without incident waves.

		$\bar{C}_T$			$\eta_{P(\%)}$
Method	Case	Fore	Aft	Tandem	Tandem
CFD	Free-surface	0.48	0.74	1.22	78.9
	Infinite	0.51	0.87	1.37	80.1
Semi-Analytical	Free-surface	0.45	0.67	1.12	76.1
	Infinite	0.39	0.59	0.98	82.6

In infinite domain configuration the aft foil mean thrust is very significantly augmented through its interaction with the fore foil wake resulting in the whole tandem having mean thrust values 2.6 times larger than the single foil, while the propulsive efficiency slightly increases both in the aft foil and in the tandem (Lopes et al. 2023a). With the free-surface the fore foil presents a slight decrease in thrust while the aft foil thrust reduction is more significant. This indicates that part of the augmentation in thrust gained by the aft foil is being lost in wave radiation. The semi-analytical model presents a fair-to-good agreement with the CFD results.

Figure 7 presents the eddy viscosity ratio, showing that turbulence occurs mainly in the wake. It is important to remark that the turbulence near the free-surface is numerical and does not translate a physical phenomenon. This might be explained by low refinement near the free-surface, causing the VOF equations to generate vorticity, which artificially creates turbulence.

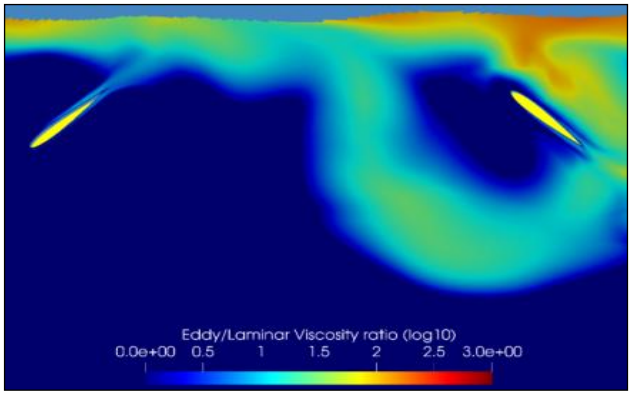

Figure 7: Eddy viscosity ratio (log scale) for the submerged tandem foil case. Laminar flow in blue and turbulent flow in red.

4.2 Tandem Foil in Heading Waves

Since there are no published studies for this case, here we present a single demonstrative case, and a preliminary discussion of the physical phenomena involved, leaving a thorough investigation of this case for future work. The simulation uses a grid of 1030k cells and number of iterations per period n_t/T = 2607. The inter foil phase lag is selected so the positive interference of the wakes can be studied. The wave and motion parameters are shown in Table 3. The motion frequency is equal to the encounter frequency.

Table 3: Simulation parameters for the tandem foil in waves.

Parameter	Value
Inflow velocity, U	0.39 m/s
Chord, c	0.1 m
Pitching axis, b^*	1/3-point
Heave amplitude, h_{oi}	1.0 m
Pitch amplitude, θ_{oi}	35°
Pitch phase, ψ_i	90°
Oscillating period, T	1.30 s
Submergence, d	0.25 m
Foil separation, s	0.4 m
Inter-foil phase lag, ϕ_t	180°
Wave amplitude, a_0	0.075 m
Wave period, T_w	1.51 s
Wave-heave phase, ϕ_w	-90°
Reynolds number, Re	40 000

Figure 8 shows a sequence of snapshots of the instantaneous vorticity and velocity fields for this test case at quarter cycle instants. It is possible to observe the alternating shedding of clockwise and anticlockwise vortices, both primary and secondary, of both fore and aft foils, as seen in the previous section. The key difference here is a significant change in the wake's pattern caused by the orbital wave velocity field. For the fore foil, in the downstroke, the secondary anticlockwise trailing edge vortex (red in colour), visible in t/T = 0.75 and t/T = 0 (previous cycle), with the motion of the wave, is drawn near and absorbed into the primary vortex (red in colour) increasing its strength. On the other side, in the upstroke, the wave causes the separation of both the fore foil primary and the secondary clockwise vortices (both in blue) between t/T=0.25 to 0.75. Thus, the secondary vortex stays between the primaries, reducing the jet velocity and the thrust. This creates a pattern of three vortices, instead of the four observed previously. Regarding the interaction of the two foils' wakes, in this case, the aft foil is weaving in between the primary vortices that are shed from the fore foil. However, because of the fore foil wake pattern change, the interaction of vortices become very complex. The interaction of the aft foil primary clockwise vortex (blue) with fore foil primary anticlockwise vortex (red) seems to cause the dissipation of both, weakening the thrust from t/T = 0.25 to 0.75. The interaction of the aft foil primary anticlockwise vortex (red) with fore foil secondary clockwise vortex (blue) appears to strengthen the first, thus increasing the thrust.

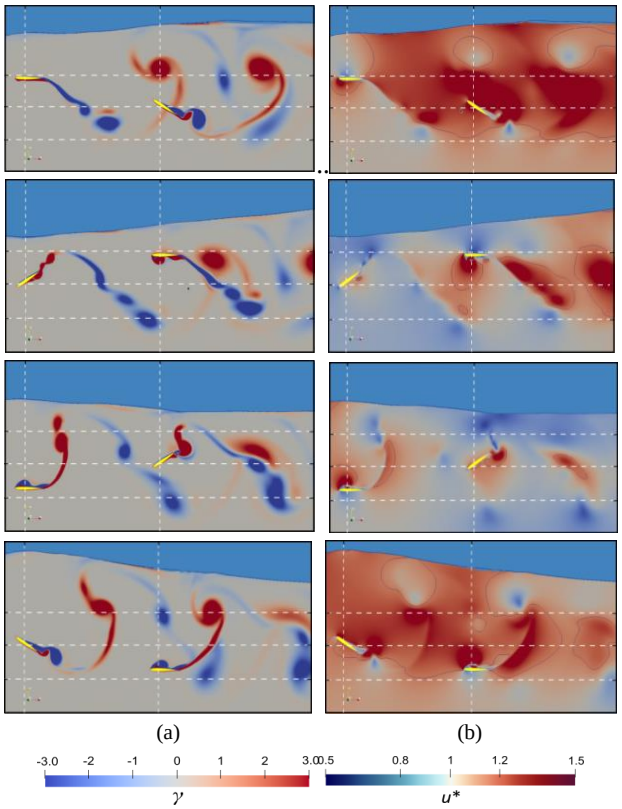

Figure 8: Snapshots of (a) vorticity and (b) normalized velocity fields contours at cycle increments of t/T = ¼, for a tandem foil oscillating in waves. Clockwise vorticity is indicated with blue, and anticlockwise with red.

In the velocity field snapshots, it is visible that the jet velocity behind the fore foil is higher with the crest and lower with the trough. During most of the rising and downing of the wave crest the velocities behind the aft foil are greatly increased, indicating that, the two foils are overall interacting positively, despite the positive and negative interferences of the different vortices just described.

Figure 9 shows the instantaneous thrust, vertical and moment coefficients for both fore and aft foils. It is possible to see the augmentation of the aft thrust relative to the fore foil and the differences in the thrust in the two parts of the cycle, where from t/T=0.5 to 0.75 the thrust becomes significantly negative, because of the effect of the fore foil secondary anticlockwise vortex.

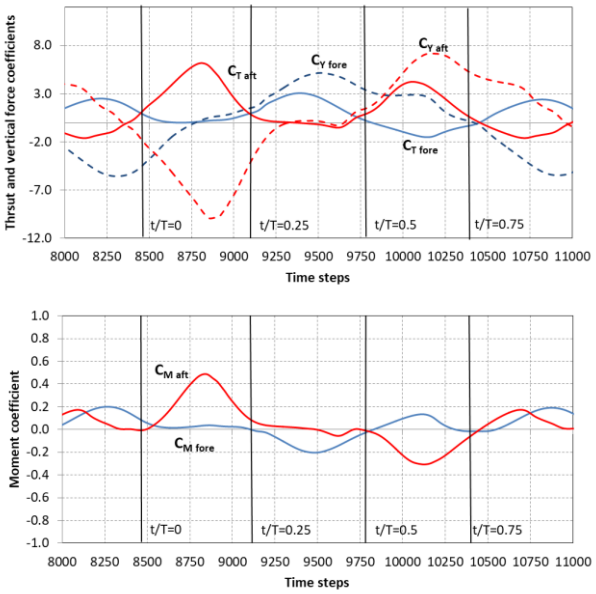

Figure 9: (a) Thrust and vertical and (b) moment coefficients instantaneous values for the forward foil and aft foil in tandem in the heading waves test case.

Table 4: Results of the average thrust coefficient and propulsive efficiency for the tandem foil in heading waves.

Method	Parameter	Fore foil	Aft foil	Tandem foil
CFD	$\bar{C}_T$	0.81	1.43	2.23
	η_p [%]	64.7	88.0	67.5
Semi-Analytical	$\bar{C}_T$	1.87	2.65	4.52
	η_p [%]	91.3	97.0	94.2

Table 4 presents the results of the average thrust coefficient and propulsive efficiency. The aft foil presents a significant increase of the average thrust, and a modest increase of the propulsive efficiency, when compared with the fore foil. The total tandem foil configuration, when compared with the sum of two isolated single/fore foils has mean thrust values 38% higher and presents just a slight increase in propulsive efficiency.

5 CONCLUSIONS

This paper presents a study on flow dynamics of tandem oscillating foil thrusters, considering cases without and with heading waves. High performance configurations are studied, when the aft foil is weaving in between the primary vortices shed by the fore foil, especially when the aft foil collides favorably with the secondary vortices shed by the fore foil, strengthening aft foil primary vortices and repositioning of the fore secondary vortices. When compared with the infinite domain case, with a free-surface without incident waves, the fore foil presents a decrease in thrust of the order of 6% while the aft foil thrust reduces about 15%.

In agreement with the conclusions of Silva et al. (2012), we observe that the problem of the oscillating foils in waves has some different features when compared to the foils in an infinite domain and calm waters. We found for the tandem foil in waves, a significant pattern change in the wake caused by the orbital wave velocity field. For the high amplitude test case studied, a wake pattern of three vortices is created, instead of four, as previously observed. One of the primary vortices is strengthened by absorbing one of the secondary vortices, and the other secondary vortex becomes more defined. This creates unevenness in the wake, reinforcing thrust in one stroke and drag in the other.

The case of the tandem foil in waves shows very promising results. The high performance configuration tested experiences increases in thrust of 38% when compared with the sum of two isolated fore foils. It reaches high thrust values of $\bar{C}_{TSA}$ = 1.11 with 67.5% propulsive efficiency. The semi-analytical model provides significant discrepancies to the numerical results. The over predictions might be explained by the losses in lift due to the full separation of the flow (Figure 8a) that are not accounted for in the model. The flow dynamics visualization obtained in this research suggests that even better performances might be possible. For example, by making the aft foil collide with the fore secondary vortex, to weaken its effect and/or by trying to avoid the unfavorable interaction of the aft secondary foil with fore main primary vortices.

With further improvements the semi-analytical model may provide a useful tool with approximate precision, suitable for use in engineering design and optimization. It presents simulation times less than one minute for the most complex test case, using a personal computer, while the CFD model calculations lasted up to 10 days using the *Iridis5* supercomputer.

ACKNOWLEDGEMENTS

The authors acknowledge the use of the IRIDIS High Performance Computing Facility, and associated support services at the University of Southampton (2022), in the completion of this work. This work was supported by Fundação para a Ciência e Tecnologia, WavEC Offshore Renewables, blueOASIS and Instituto Superior Técnico, Lisbon.

REFERENCES

Balay, S., Abhyankar, S., Adams, M.F., Brown, J., Brune, P., Buschelman, K., Dalcin, L., Dener, A., Eijkhout, V., Gropp, W.D., Karpeyev, D., Kaushik, D., Knepley, M.G., May, D.A., McInnes, L.C., Mills, R.T., Munson, T., Rupp, K., Sanan, P., Smith, B.F., Zampini, S., Zhang, H. and Zhang, H. 2020. PETSc Users Manual. Technical Report ANL-95/11 Revision 3.13, Argonne National Laboratory.

Belibassakis, K.A. & Filippas, E.S. 2015. Ship propulsion in waves by actively controlled flapping foils. Appl. Ocean Res. 52, 1–11.

Bøckmann, E. & Steen, S. 2013. The effect of a fixed foil on ship propulsion and motions. Proceedings of the Third International Symposium on Marine Propulsors, 553–561.

Bøckmann, E. & Steen, S. 2014. Experiments with actively pitch-controlled and springloaded oscillating foils. Appl. Ocean Res. 48, 227–235.

Bøckmann, E. & Steen, S., 2016. Model test and simulation of a ship with wavefoils. Appl.Ocean Res. 57, 8–18.

Deng, J., Shao, X.M. and Yu, Z.S. 2007. Hydrodynamic studies of two wavy foils in tandem arrangement. Physics of Fluids 19, 113104.

Eça, L. & Hoekstra, M. 2014. A procedure for the estimation of the numerical uncertainty of CFD calculations based on grid refinement studies. Journal of Computational Physics 262, 104–130.

Faltinsen, O.M. 2005. Hydrodynamics of High-Speed Marine Vehicles. Cambridge University Press.

Fernandes, G., Kapsenberg, G.K., Kerkvliet, M. and Walree, F. van 2016. Towards Accurate Computations of Active Stabiliser Fins, focusing on Dynamic Stall. 15th International Ship Stability Workshop, 51-58, Stockholm, Sweden

Ferziger, J.H. & Perić, M. 2002. Computational Methods for Fluid Dynamics, 3rd edition. Berlin. Springer-Verlag.

Filippas, E.S., Gerostathis, T.P. and Belibassakis, K.A., 2018. Semi-activated oscillating hydrofoil as a nearshore biomimetic energy system in waves and currents. Ocean Eng. 154, 396–415.

Hoerner, S.F. 1965, Fluid Dynamic Drag. Hoerner Fluid Dynamics, Bricktown, New Jersey.

Isshiki, H. 1982a. A theory of wave devouring propulsion (1st Report). Thrust Generation by a Linear Wells Turbine. J. Soc. Nav. Archit. Jpn. 151, 54–64.

Isshiki, H. 1982b. A theory of wave devouring propulsion (2st Report). Optimized foil motions for a passive-type wave devouring propulsion. J. Soc. Nav. Archit. Jpn. 151, 54–64.

Isshiki, H. & Murakami, M. 1983. A theory of wave devouring propulsion (3rd report). An experimental verification of thrust generation by a passive-type hydrofoil propulsor. J. Soc. Nav. Arch. Japan 154, 125

Isshiki, H. & Murakami, M. 1984. A theory of wave devouring propulsion (4th Report): A comparison between theory and experiment in case of a passive-type hydrofoil propulsor. J. Society of Naval Architects of Japan 156, 102–114.

Joshi V. & Mysa R.C. 2021. Mechanism of wake-induced flow dynamics in tandem flapping foils: Effect of the chord and gap ratios on propulsion. Phys. Fluids *33*, 087104.

Klaij, C., Hoekstra, M. and Vaz, G. 2018. Design, analysis and verification of a Volume-of-Fluid model with interface-capturing scheme. Computers and Fluids 170, 324–340.

Lagolopoulos N., Weymouth G. and Ganapathisubramani B. 2020. Deflected Wake Interaction of Tandem Flapping Foils. Journal of Fluid Mechanics 903, A9.

Lighthill, M. J. 1960. Note on the swimming of slender fish. J. Fluid Mech 9 (02), 305-317.

Lombardi M., Parolini N. and Quarteroni A. 2013. Radial basis functions for inter-grid interpolation and mesh motion in FSI problems. Computer Methods in Applied Mechanics and Engineering 256, 117-131.

Lopes, D.B.S. 2022. On the Modelling of Oscillating Foils for Wave Propulsion, PhD thesis, Instituto Superior Técnico, Universidade de Lisboa, Portugal

Lopes, D.B.S., Vaz, G., Campos, J.A.C. and Sarmento, A.J.N.A. 2023a. Analytical and numerical modelling of tandem oscillating foils propulsors. Ocean Engineering 270.

Lopes, D.B.S., Vaz, G., Campos, J.A.C. and Sarmento, A.J.N.A. 2023b. Modelling of oscillating foil propulsors in waves. Ocean Engineering 268.

Menter F.R., Kuntz, M. and Langtry, R. 2003. Ten Years of Industrial Experience with the SST Turbulence Model. Proceedings of the 4th Turbulence, Heat and Mass Transfer, 625-632.

Mewes, S. 2021. Numerical Prediction of Hydrodynamic Loads and Damping of a Floating Offshore Wind Turbine. PhD thesis, Universität Duisburg-Essen. Germany.

Moukalled, F., Mangnani, L., and Darwish, M. 2016. The Finite Volume Method in Computational Fluid Dynamics. Springer International Publishing.

Muscutt, L., Ganapathisubramani, B., and Weymouth, G. 2014 Characteristics of the flow around tandem flapping wings. Bulletin of the American Physical Society 59.

Newman, J. N. 1978. Marine Hydrodynamics. Cambridge, MIT Press.

Numeca, 2022. (https://www.numeca.com/hexpress).

Patankar, S. 1980. Numerical Heat Transfer and Fluid Flow. Routledge.

Pereira, F. 2018. Towards Predictive Scale-Resolving Simulations of Turbulent External Flows. PhD thesis, Instituto Superior Técnico, Lisboa, Portugal.

Perić, R. & Abdel-Maksoud, M. 2016. Reliable damping of free-surface waves in numerical simulations. Ship Technology Research – Schiffstechnik 63.

ReFRESCO, 2022. (https://www.refresco.org)

Roe, P. L. 1985. Some contributions to the modelling of discontinuous flows. Lectures in Applied Math 22, 163-193.

Schlichting H. & Gersten K. 2017. Boundary Layer Theory (9th edition), Springer-Verlag.

Skjelbreia, L. & Hendrickson, J. 1960. Fifth order gravity wave theory. Proc. Coastal Engineering Conf., 184-196.

Silva, L.W.A.D. & Yamaguchi, H. 2012. Numerical study on active wave devouring propulsion, Journal Marine Science & Technology 17(3), 261-275.

Theodorsen, T. 1935. General theory of aerodynamic instability and the mechanism of flutter. NACA Tech. Rep. 496.

University of Southampton, 2022. The Iridis Compute Cluster (https://www.southampton.ac.uk/isolutions/staff/iridis.page)

Vaz, G., Jaouen, F. and Hoekstra, M. 2009. Free-Surface Viscous Flow Computations. Validation of URANS code FreSCo, OMAE2009, Hawaii, Honolulu, USA.

Wu, T.Y. 1971. Hydromechanics of swimming propulsion (Part 2): Some optimum shape problems. J Fluid Mech 46, 521–544.

Wu, T.Y. & Chang, A.T. 1975. Extraction of flow energy by fish and birds in a wavy stream. Swimming and flying in nature. Springer, 687-702.

Wu, X., Zhang X., Tian, X., Li, X. and Lu W. 2020. A review on fluid dynamics of flapping foils. Ocean Engineering 195, 106712.

Xie, H., Wang, D., Lin, Z., Qiu, S., & Jiawei Y. 2017. Hydrodynamic Performance of Tandem Oscillating Foils in Waves. 27th International Ocean and Polar Engineering Conference, San Francisco.

Zhu, Q., 2012. Energy harvesting by a purely passive flapping foil from shear flows. Journal of Fluids and Structures 34, 157–169.